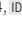


Replication

[Re] A circuit model of auditory cortexParvathy Neelakandan¹ and Christoph Metzner^{1,2,3,4, }

¹Neural Information Processing Group, Technische Universität Berlin, Berlin, Germany – ²Department of Child and Adolescent Psychiatry, Charité–Universitätsmedizin Berlin, Berlin, Germany – ³Institute for Robotics and Cognitive Systems, Universität zu Lübeck, Lübeck, Germany – ⁴Biocomputation Research Group, School of Physics, Engineering and Computer Science, University of Hertfordshire, Hatfield, United Kingdom

Edited by
(Editor)

Reviewed by
(Reviewer 1)
(Reviewer 2)

Received
–

Published
–

DOI
–

Introduction

In this work, we successfully replicated the results of the rate models in the article *A circuit model of auditory cortex* written by Youngmin Park and Maria N. Geffen [1]. This replication has been done using Python, and the code is available on GitHub [empty citation]. In this replication, we focus on the rate models proposed in the original article and have not attempted to replicate the spiking network models. We focus on the rate models because of a) their simplicity, b) the fact that the rate equations were solved using XPPAUT [2], a tool that, despite its history and usefulness, many neuroscientists might be less familiar with than a pure Python implementation and c) because the rate models could be easily included in the whole-brain models, for example with the Python package *neurolib* [3] developed in our group. With minor parameter tweaking, they may serve as a generic building block for regional brain dynamics with two inhibitory populations. In their article, Park and Geffen propose 1) an extended Wilson-Cowan model, consisting of one excitatory and two inhibitory populations and 2) use this model in different settings to explore a broad set of experimental findings in auditory cortex.

1) The extended Wilson-Cowan model describes three populations of neurons that represent excitatory pyramidal neurons (Exc), parvalbumin-positive inhibitory interneurons (PV) and somatostatin-positive inhibitory interneurons (SST). The model further includes currents that represent the optogenetic activation or silencing of the two inhibitory populations. This extended model is then employed in two different settings, a single-unit model representing a piece of auditory cortex preferring a single tone frequency and a three-unit model representing a piece of cortex comprised of three regions with different frequency preferences, set up in a tonotopic fashion.

2) The experimental experiments range from stimulus-specific adaptation experiments using oddball sequences over forward suppression experiments to feedforward functional connectivity experiments.

In the Methods section we provide details on the two different versions of the rate model, the single-unit and the three-unit model. In the Results section we then compare our replication to the original model on the three types of experiments mentioned above.

Methods

The firing rate model from the original article was an extension of the traditional Wilson-Cowan model [4] and represented an iso-frequency unit of the auditory cortex. This

Copyright © 2022 P. Neelakandan and C. Metzner, released under a Creative Commons Attribution 4.0 International license.

Correspondence should be addressed to Christoph Metzner (cmetzner@ni.tu-berlin.de)

The authors have declared that no competing interests exists.

Code is available at <https://github.com/rescience-c/template>.

Open peer review is available at https://github.com/ChristophMetzner/ReScience_ReplicationParkGeffen.

iso-frequency unit consisted of one excitatory and two inhibitory populations. Building on this unit a more complex three-unit rate models was developed, to investigate stimulus-specific adaptation, forward suppression, tuning-curve adaptation and feedforward functional connectivity.

Iso-Frequency Unit Model The iso-frequency unit model was based on the Wilson-Cowan model [4] but was modified to include two different types of inhibitory interneurons. The two inhibitory population are meant to represent parvalbumin-positive (PV) and somatostatin-positive (SST) cells. The single unit model is given by

$$\tau_u \frac{du(t)}{dt} = -u(t) + f(w_{ee}u(t) - w_{ep}p(t) - w_{es}s(t) + qg(t)i(t)), \quad (1)$$

$$\tau_p \frac{dp(t)}{dt} = -p(t) + f(w_{pe}u(t) - w_{pp}p(t) - w_{ps}s(t) + I_{Opt,PV}(t) + qg(t)i(t)), \quad (2)$$

$$\tau_s \frac{ds(t)}{dt} = -s(t) + f(w_{se}u(t) - w_{sp}p(t) - w_{ss}s(t) + I_{Opt,SST}(t)), \quad (3)$$

with $u(t)$, $p(t)$, and $s(t)$ being the normalized firing rates (in $[0, 1]$) of the pyramidal cell population, the PV population and the SST population, respectively. Furthermore, w_{xy} represents the strengths of connections from population y to population x . The two terms $I_{Opt,PV}$ and $I_{Opt,SST}$ describe the input current to cells due to optogenetic stimulation of the PV population and SST population, respectively. $\tau_i, i \in u, p, s$ defines the time constants for the respective populations. The function f is realised as a threshold linear function given by

$$f(x) = \begin{cases} 0 & \text{if } x \leq 0 \\ rx & \text{if } 0 < x \leq 1/r \\ 1 & \text{if } x > 1/r, \end{cases}$$

(4)

which coarsely approximates a sigmoid function. Furthermore, the function f is thresholded by simply subtracting a constant u_i from the input x (i.e. $f(x - u_i)$) which varied for the different populations. Lastly, afferent auditory input fed into the unit is given by $qg(t)i(t)$, which is subdivided into the 'raw' input $i(t)$ and a slow modulation $g(t)$ mimicking synaptic depression at thalamic synapses. The input function $i(t)$ is simply an instantaneous rise with amplitude q and an exponential decay with a time constant of τ_q . The synaptic depression $g(t)$ is governed by the following equation

$$\frac{dg(t)}{dt} = \frac{g_0 - g(t)}{\tau_{d1}} - \frac{g(t)i(t)}{\tau_{d2}}. \quad (5)$$

The parameter values can be found in Table 1

Three-Unit Model Building on the single unit model a three-unit model was implemented, with each single unit representing a different input frequency, thus creating a simple tonotopic layout that allowed to explore more complex auditory inputs. Intra-unit connectivity was as described before for the single-unit model. Inter-unit connectivity was restricted to immediate neighbours and included the following connection types: Exc to exc, exc to PV and SST to exc. Together, the activity of the three populations of each unit was governed by

$$\tau_u \frac{du_i(t)}{dt} = -u_i(t) + f(w_{ee}u_i(t) - (w_{ep} - a(1 - D_i(t)))p_i(t) - w_{es}s_i(t) + J_{1,i}(t)), \quad (6)$$

Table 1. Overview of the model parameters for the single unit model.

Parameter	Symbol	Value
<i>Time constants</i>		
E membrane time constant	τ_u	10 ms
PV membrane time constant	τ_p	10 ms
SST membrane time constant	τ_s	10 ms
Input time constant	τ_q	10 ms
STP replenishment time constant	τ_{d1}	1,500 ms
STP depletion time constant	τ_{d2}	20 ms
<i>Weights</i>		
E-E coupling	w_{ee}	1.1
E-PV coupling	w_{ep}	2.0
E-SST coupling	w_{es}	1.0
PV-E coupling	w_{pe}	1.0
PV-PV coupling	w_{pp}	2.0
PV-SST coupling	w_{ps}	2.0
SST-E coupling	w_{se}	6.0
SST-PV coupling	w_{sp}	0.0
SST-SST coupling	w_{ss}	0.0
<i>Gains</i>		
E gain	r_u	3.0
PV gain	r_p	3.0
SST gain	r_s	3.0
<i>Thresholds</i>		
E threshold	u_th	0.7
PV threshold	p_th	1.0
SST threshold	s_th	1.0
<i>Synaptic depression</i>		
Baseline	g_0	1.0
<i>Input</i>		
Input amplitude		5.0
<i>Optogenetic currents</i>		
PV (in-)activation current	$I_{Opt,PV}$	-2.
SST (in-)activation current	$I_{Opt,SST}$	-1.

$$\tau_p \frac{dp_i(t)}{dt} = -p_i(t) + f(w_{pe}u_i(t) - w_{pp}p_i(t) - w_{ps}s_i(t) + I_{Opt,PV}(t) + J_{2,i}(t)), \quad (7)$$

$$\tau_s \frac{ds_i(t)}{dt} = -s_i(t) + f(w_{se}u_i(t) - w_{sp}p_i(t) - w_{ss}s_i(t) + I_{Opt,SST}(t) + J_{3,i}(t)), \quad (8)$$

with

$$J_{1,i}(t) = \begin{cases} -F_i(t)s_2(t) + qI_i(t) + w_{ee}^*u_2(t) & \text{if } i = 1, 3 \\ -F_s(t)(s_1(t) + s_3(t)) + qI_2(t) + \frac{w_{ee}^*(u_1(t)+u_3(t))}{2} & \text{if } i = 2 \end{cases} \quad (9)$$

and

$$J_{2,i}(t) = \begin{cases} qI_i(t) + w_{pe}^*u_2(t) & \text{if } i = 1, 3 \\ qI_2(t) + \frac{w_{pe}^*(u_1(t)+u_3(t))}{2} & \text{if } i = 2 \end{cases} \quad (10)$$

and

$$J_{3,i}(t) = \begin{cases} qI_i(t) + w_{se}^*u_2(t) & \text{if } i = 1, 3 \\ qI_2(t) + \frac{w_{se}^*(u_1(t)+u_3(t))}{2} & \text{if } i = 2. \end{cases} \quad (11)$$

Here, $I_i(t)$ is described by

$$I_k(t) = g_k(t)i_k(t) + g_2(t)i_2(t)\alpha \quad \text{for } k = 1, 3 \quad (12)$$

and

$$I_2(t) = (g_1(t)i_1(t) + g_3(t)i_3(t))\alpha + g_2(t)i_2(t). \quad (13)$$

Furthermore, $i_k(t)$ represents thalamic inputs to each of the three units. Taken together, the description of the three-unit model is the same than for the single-unit model, except for the addition of lateral inter-unit connectivity and short-term synaptic dynamics. Short-term facilitation is modelled by $F_i(t)$ and increases from 0 to positive values whereas depression is modelled by $D_i(t)$, which decreases from 1 towards 0. Facilitating synapses were added to Exc to SST inputs and depressing terms to PV to Exc synapses (see [5]). The facilitating term $F_j(t)$ obeys

$$\frac{dF_j(t)}{dt} = -\frac{F_j(t)}{\tau_{D_1}} + \frac{i_j(t)}{\tau_{D_2}}, \quad (14)$$

where τ_{D_1} and τ_{D_2} are again the depression time constants from the input functions of the single-unit model given in Equation 5. Analogously, the depression term $D_j(t)$ follows

$$\frac{dD_j(t)}{dt} = \frac{1 - D_j(t)}{\tau_{D_1}} - \frac{D_j(t)i_j(t)}{\tau_{D_2}}. \quad (15)$$

The choices for the parameters can be found in Table 2 and were based on experimental studies [6, 7, 8].

Park and Geffen note that, when matching model behaviour to experimental findings, two distinct parameter sets emerged and a unified rate model description required a paradigm-dependent baseline inhibition, which reflected high thalamic activity (corresponding to weak baseline inhibition) versus low thalamic activity (corresponding to strong baseline inhibition). This was implemented using another variable \bar{F} governed by

$$\frac{d\bar{F}(t)}{dt} = \frac{\bar{F}^2(t)}{\tau_{F_1}} - \frac{\bar{I}(t)}{\tau_{F_2}}. \quad (16)$$

where $\bar{I}(t)$ is the total thalamic input over all frequencies and the parameters are $\tau_{F_1} = 1500$ and $\tau_{F_2} = 100$. The function $\bar{F}(t)$ saturates to different values depending on the stimulus duration, stimulus interval and inter-trial interval. Therefore, Park and Geffen chose to set a threshold for $\bar{F}(t) = 0.22$ and distinguish two different regimes: If $\bar{F}(t)$ was above the threshold, the system is in the weak baseline inhibition regime with parameters as specified before. If however, $\bar{F}(t)$ is below the threshold the system is in the

strong baseline inhibition regime and the weights and thresholds are set to the second values in table 2.

SSA and forward suppression experiments belonged to the weak inhibitory regime and tuning-curve adaptation and PV activation belonged to the strong inhibitory regime. **ToDo: Check experiments included here**

Table 2. Overview of the model parameters for the three unit model.

Parameter	Symbol	Value
<i>Time constants</i>		
E membrane time constant	τ_u	10 ms
PV membrane time constant	τ_p	10 ms
SST membrane time constant	τ_s	10 ms
Input time constant	τ_q	10 ms
STP replenishment time constant	τ_{d1}	1,500 ms
STP depletion time constant	τ_{d2}	20 ms
<i>Weights - weak regime/strong regime</i>		
E-E coupling	w_{ee}	1.1/1.1
E-PV coupling	w_{ep}	2.0/3.0
E-SST coupling	w_{es}	1.0/3.0
PV-E coupling	w_{pe}	1.0/1.0
PV-PV coupling	w_{pp}	2.0/2.0
PV-SST coupling	w_{ps}	2.0/2.0
SST-E coupling	w_{se}	6.0/6.0
SST-PV coupling	w_{sp}	0.0/0.0
SST-SST coupling	w_{ss}	0.0/0.0
<i>Gains</i>		
E gain	r_u	3.0
PV gain	r_p	3.0
SST gain	r_s	3.0
<i>Thresholds - weak regime/strong regime</i>		
E threshold	u_th	0.7/0.7
PV threshold	p_th	1.0/1.0
SST threshold	s_th	1.0/0.0
<i>Synaptic depression</i>		
Baseline	g_0	1.0
<i>Input</i>		
Input amplitude		5.0
<i>Optogenetic currents</i>		
PV (in-)activation current	$I_{Opt,PV}$	-2.
SST (in-)activation current	$I_{Opt,SST}$	-1.

Results

Response profile of the single-unit model

Figure 1 compares the input and response profile the reproduced single-unit model, replicating Figure 1B from the original article. Qualitatively both models behave similarly, however, a quantitative difference can be noticed for the input depression variable. In our replication model g drops below 0.2 shortly after stimulus onset while in the original model g only reaches a value of ~ 0.7 . Interestingly, this did not have a visible effect on the activity rates of the three neuron types.

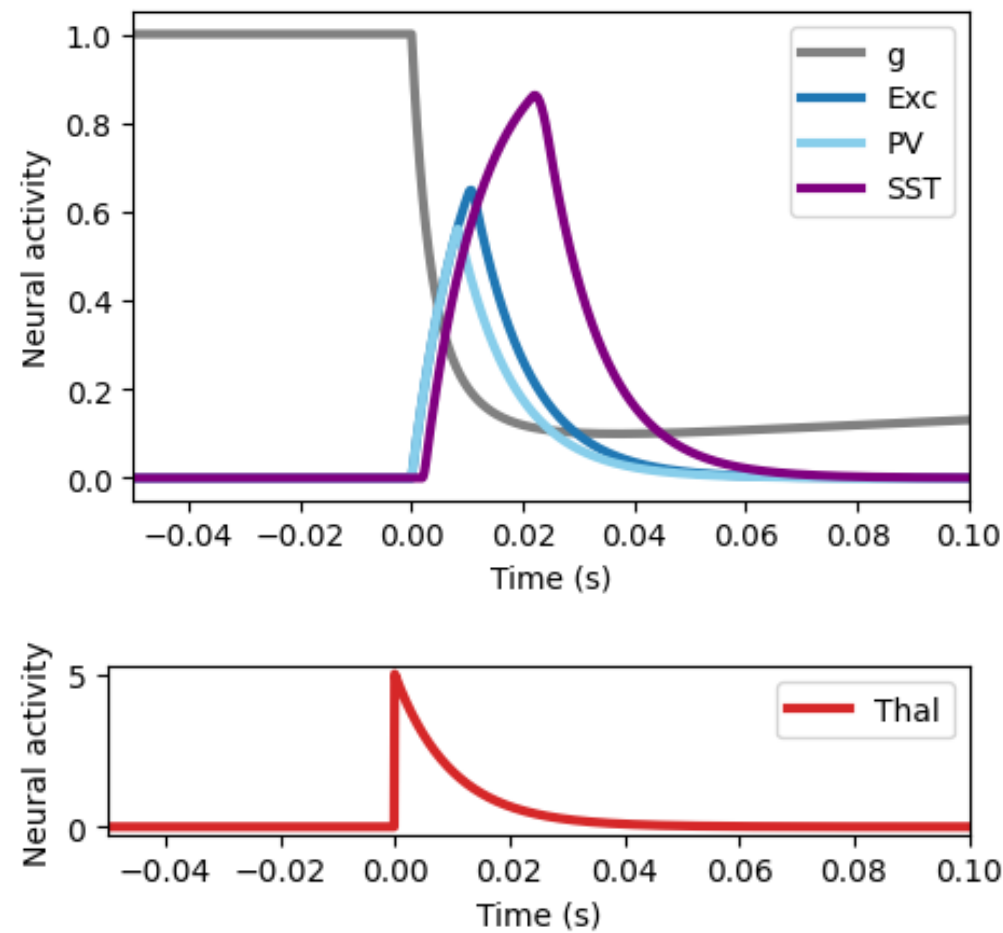


Figure 1. Replicates Figure 1B.

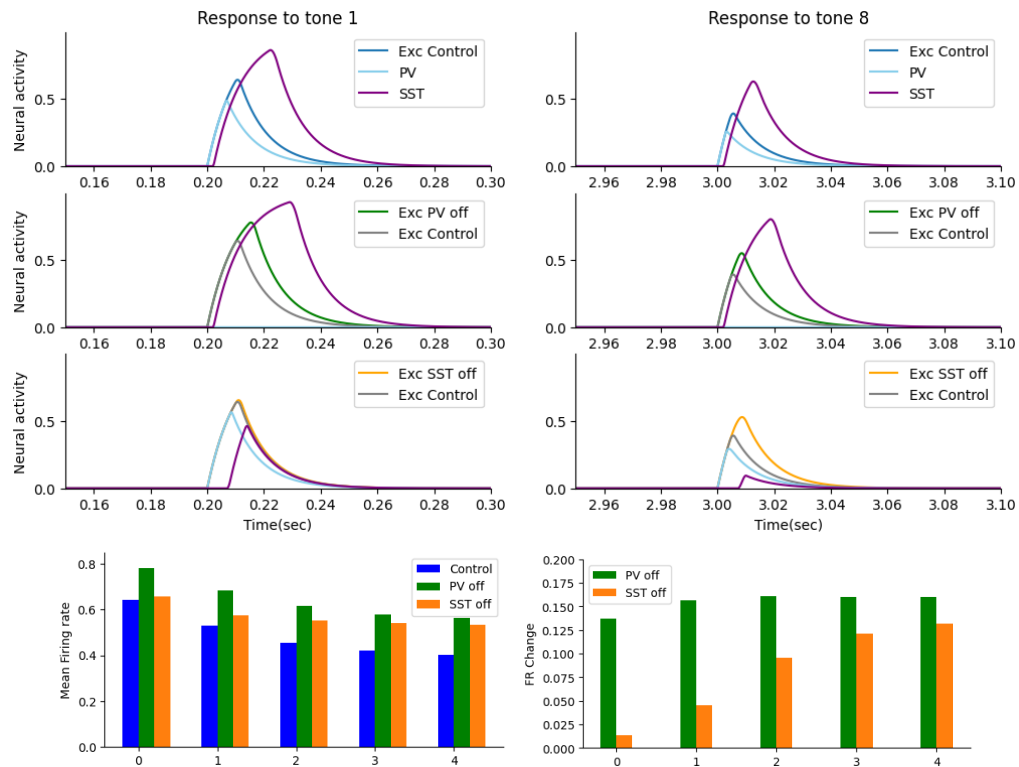


Figure 2. ReFig3: The effect of optogenetic manipulations on adaptation to repeated tones. a) Response of the three cell populations to the first (left column) and the eighth tone (right column) of the sequence for different conditions. Top row: Control condition, no optogenetic suppression. Response profile for Exc (blue), PV (light blue) and SST (magenta). Middle row: PV-Off condition, PV response was optogenetically suppressed. Response profile of Exc under PV suppression (green) and Exc in the control condition (grey), SST activity (magenta) and PV (light blue; note that they are silenced in this condition). Bottom row: SST-Off condition, SST response was optogenetically suppressed. Response profile of Exc under SST suppression (orange) and Exc in the control condition (grey), SST activity (magenta; note that the SST response was suppressed in this condition) and PV (light blue). b) Mean response of the excitatory population to the repeated tones in the three different conditions. Control (blue), PV-Off (green) and SST-Off (orange). c) Difference of excitatory responses with and without optogenetic stimulation for the two stimulation conditions. Again, PV-Off (green) and SST-Off (orange).

Differential effects of interneuron suppression in stimulus-specific adaptation

Park&Geffen first explore the differential effects of optogenetically silencing the two interneuron subtypes on stimulus-specific adaptation (SSA). To this end, the single-unit model is stimulated with 8 successive tones in three different conditions: 1) a control condition showing SSA qualitatively matching experiments [9], 2) a condition, where PV cells are optogenetically silenced and 3) one, where SST cells are silenced. The silencing currents are switched on 100 ms before tone onset and switched off 100 ms after tone onset. Each tone has a duration of 50 ms and the inter-stimulus interval is 300 ms. Figure 2 shows the results of this experiment in our replication of the single-unit model, replicating Figure 3 from the original model.

Our results qualitatively match the original model result for this experiment. First, we also see that PVs respond fastest to the tone, reaching their peak first, followed by Exc and then SSTs, which show a prominent delay caused by the indirect excitation of SSTs through Exc (Figure 2 a)). As in the original model, this faster response of PVs results in them immediately affecting the Exc population and, therefore, changes to PVs directly

translate to changes in Exc activity. Changed SST activity only influences Exc activity with a substantial delay.

Therefore, PV suppression directly leads to increases in Exc activity. Furthermore, it leads to a disinhibition of SSTs because of the increased Exc activity and the reduced inhibition from PVs. However, the resulting increase in SST-induced inhibition of Exc is not sufficient to compensate for this increased Exc activity. As a consequence, the Exc population responds with increased activity for all tones of the sequence as a result of this relatively constant disinhibition (Figure 2 b) and c)).

SST suppression, on the other hand, initially does not affect Exc because of the temporal profile of SST activity and the fact that PVs can compensate for the reduced SST activity. After adaptation, which causes an overall decrease in excitatory activity (from Exc but also from thalamus) and thus reduced PV activity, the Exc population experiences a net loss of inhibitory current. This resulted in a successive increase of disinhibition over the course of the sequence (Figure 2 b) and c)). As in the original model, the differential roles the two interneuron populations play can be understood in terms of this simple disinhibition and compensation mechanism.

Qualitatively, our results match those from the original study very well and also the temporal profiles of the populations seem almost identical. The amplitudes of the responses, however, do not match. In our understanding the amplitude of the extended Wilson-Cowan model should not exceed 1, which it does in the original model.

The second experiment in the original manuscript, explores the model dynamics in a three-unit model, where each unit represents a different frequency. In an oddball paradigm, the standard (shown 90% of the time) and the deviant stimulus (shown 10% of the time) activate the unit left and right to the central unit, respectively, whose activity is measured. Again, three conditions are explored, the control condition with no optogenetic manipulations and two conditions where the PV and the SST populations are optogenetically manipulated, respectively. As before, optogenetic stimulation is turned on a 100 ms before tone onset and turned off 100 ms after onset. Additionally to suppression of the interneuron populations, trying to replicate the experimental findings from Natan et al. [9], Park and Geffen also generate predictions for the effect an activation of the interneurons would have by injecting an activating current.

Similar to the original model, in our model the firing rates increased to all post-deviant tones, however, in different ways for the two optogenetic manipulations (Figure 3 (a)). Silencing PV cells led to a relatively uniform increase across all tones independent of the distance to the deviant. For the SST-Off condition firing rates increased more with growing distance to the deviant tone, again replicating the experimental findings from Natan et al. [9]. Our model also generates the same predictions in response to the oddball stimulus for optogenetic activation of PV and SST cells, respectively (3 (b)). Here, we saw that activation of PV cells uniformly decreased the post-deviant response, while SST activation decreased activity dependent on the distance to the deviant stimulus.

Following this, Park and Geffen explored the robustness of their stimulus-specific adaptation results. They explored four parameters that they hypothesized to be crucial to mediate adaptation. The first parameter, the weight w_{ee} of recurrent excitation, is considered a key parameter [10] and has been found important in inhibitory-stabilized networks [6, 11]. The second parameter was the timescale of thalamic depression τ_{d1} , because the range of experimentally measured values varies greatly [9, 10]. Lastly, they manipulated the strength of optogenetic PV modulation and the strength of optogenetic SST modulation, respectively. To assess the strength of adaptation, they used the Common-contrast SSA Index (CSI)

$$CSI = \frac{d(f_1) + d(f_2) - s(f_1) - s(f_2)}{d(f_1) + d(f_2) + s(f_1) + s(f_2)} \quad (17)$$

where $d(f_i)$ is the deviant rate response and $s(f_i)$ is the standard rate response to frequency f_i . A $CSI = 1$ indicates full adaptation, whereas a $CSI = 0$, which means that standard deviant responses are equally strong, indicates weak SSA.

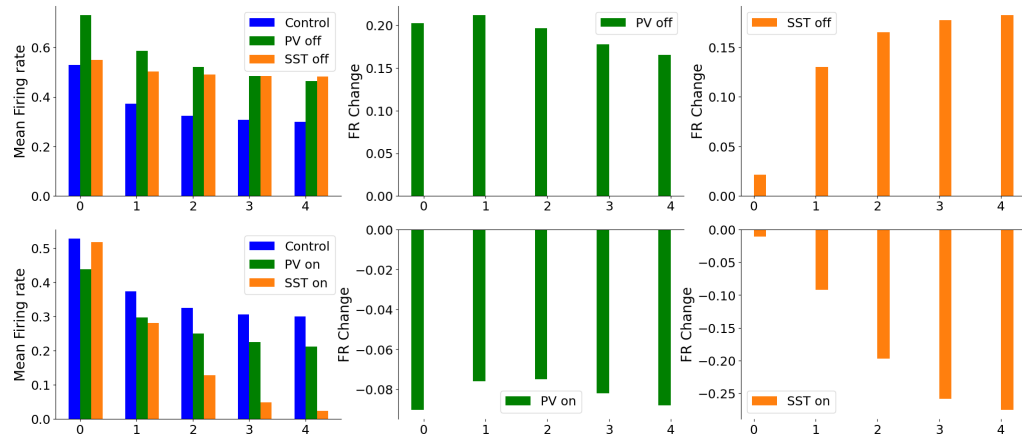


Figure 3. ReFig4: Summary of SSA in the rate model. Response of the three-unit model to an odd-ball stimulus consisting of standard tones (appearing with 90% probability) and deviant tones (appearing with 10% probability). Standard tones were presented to unit 1 and deviant tones to unit 3. Responses were measured in the middle unit 2. a) Suppression: Left: Average response of the excitatory population to the control condition (no optogenetic stimulation; blue), the PV-Off condition (optogenetic suppression of PV cells; green) and the SST-Off condition (optogenetic suppression of SST cells; orange). Middle: Firing rate change PV-Off condition versus control condition. Right: Firing rate change SST-Off condition versus control condition. b) Activation: Left: Average response of the excitatory population to the control condition (no optogenetic stimulation; blue), the PV-On condition (optogenetic activation of PV cells; green) and the SST-On condition (optogenetic activation of SST cells; orange). Middle: Firing rate change PV-On condition versus control condition. Right: Firing rate change SST-On condition versus control condition.

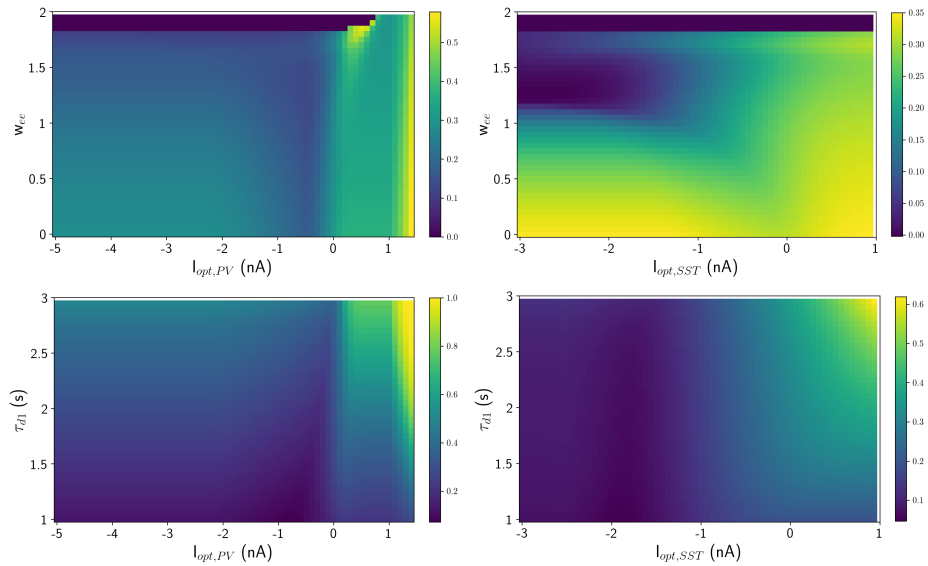


Figure 4. ReFig5: Predicted effects of the key parameters on the common-contrast SSA index. Top left: PV optogenetic parameter ($I_{opt,PV}$) vs. recurrent excitation (w_{ee}). Top right: SST optogenetic parameter ($I_{opt,SST}$) vs. recurrent excitation (w_{ee}). Bottom left: PV optogenetic parameter ($I_{opt,PV}$) vs. thalamic depression time constant (τ_{d1}). Bottom right: SST optogenetic parameter ($I_{opt,SST}$) vs. thalamic depression time constant (τ_{d1}).

Figure 4 shows the results of the parameter sweeps in our model replication. Similar to the results from the original study, CSI did not change strongly when varying w_{ee} and τ_{d1} for a fixed strength of optogenetic modulation, suggesting that the model is not sensitive to moderate changes of these parameters and that normal function seems not to depend on their fine tuning.

Differential effects of inhibitory neuron manipulation on cortical forward suppression

A well-described example of context dependence in auditory cortex is the so-called ‘forward suppression’, where the response of neurons to a tone (the probe) is reduced by a preceding different tone (the masker). Furthermore, the strength of suppression depends on the frequency difference between the tones. While forward suppression was thought to be explained by a depression of feedforward synapses, Phillips et al. [12] recently demonstrated the involvement of inhibitory interneurons in this phenomenon. PV suppression led to a selective increase of forward suppression at the preferred frequency of the neuron relative to control, whereas SST inactivation reduced forward suppression relative to control.

Park and Geffen reproduce this experiment in their three-unit model by applying a masker tone to either the 1st, 2nd or 3rd unit and a probe tone to the 2nd, where the response is measured. Masker and probe are both 50 ms long and separated by an inter-stimulus interval of 20 ms. In both optogenetic manipulation conditions the manipulation is present throughout the trial. As in the experimental study, in their model PV inactivation leads to a selective increase of forward suppression and SST inactivation to a selective decrease of forward suppression. Park and Geffen also generate model predictions in response to an activation of PV and SST cells, respectively. Both manipulations led to an increase in forward suppression for the preferred frequency but also for the two frequencies next to it.

Figure 5 shows the results of this experiment with our model. Our model reproduced the selective increase of forward suppression in the PV-Off condition and the selective decrease of suppression in the SST-Off condition. We could, however, not reproduce the model predictions. Our model predicts a selective increase of forward suppression at the preferred frequency but no change at the other two frequencies in the PV-Off condition.

PVs enhance feedforward functional connectivity

Park and Geffen also explore the role of PV cells in feedforward functional connectivity in their model. Following the experimental study from Hamilton et al. [13], which found an increase of thalamo-cortical coupling after PV cell activation, they explore this in their model and hypothesize that a sharpening of cortical responses upon PV cell activation would align the responses more closely with the thalamic inputs and would thus improve feedforward functional connectivity.

To test this hypothesis, they stimulated the 2nd unit of the three-unit model with a single tone in two conditions, a control condition without any optogenetic manipulation and a PV-On condition with optogenetic activation of PV cells.

Replicating the original results, we found that activation of PV interneurons resulted in an decrease of activity and an increase in the correlation between thalamic and cortical response (see Figure 6 left panel). Furthermore, an inactivation of PV cells increased the response and led to a further decoupling of cortical and thalamic responses (see Figure 6 right panel).

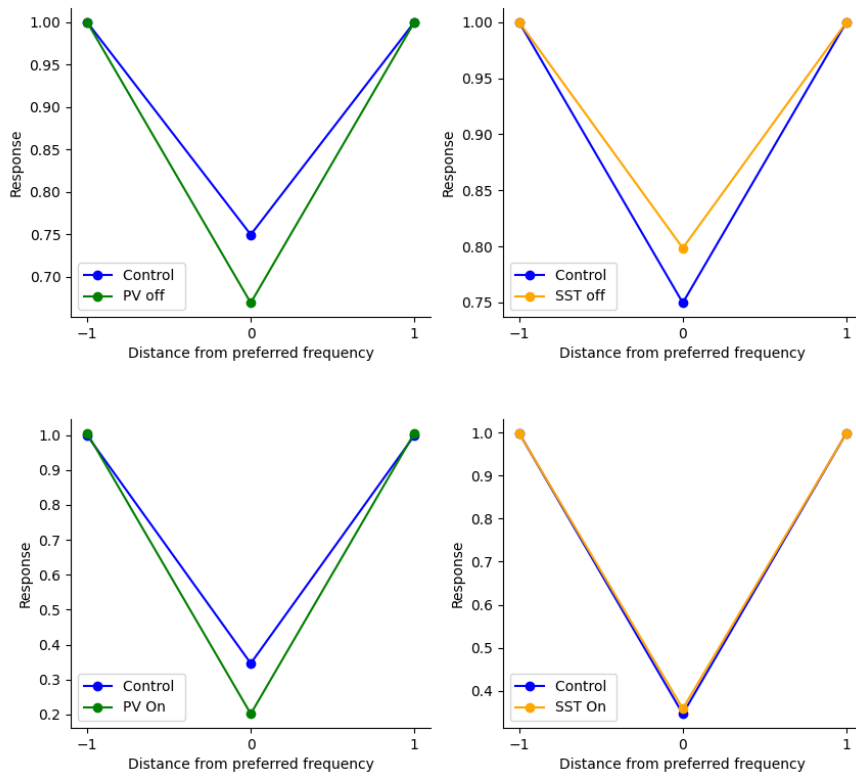


Figure 5. ReFig6: Forward suppression in the rate model (Parameters from the table). The forward suppression stimulus consists of two successive tones. The first tone activates the 1st, 2nd or 3rd unit, whereas the second tone always activates the 2nd unit in the middle. This creates two conditions, where the first tone (masker) either activates a neighbouring frequency (if the 1st and 3rd unit are activated) or the same frequency (if the 2nd unit is activated) as the second tone (the probe). a) Response of the 2nd unit for the three different trials in the control condition and the PV-Off condition (left column) or the SST-Off condition (right column). b) Response of the 2nd unit for the three different trials in the control condition and the PV-On condition (left column) or the SST-On condition (right column).

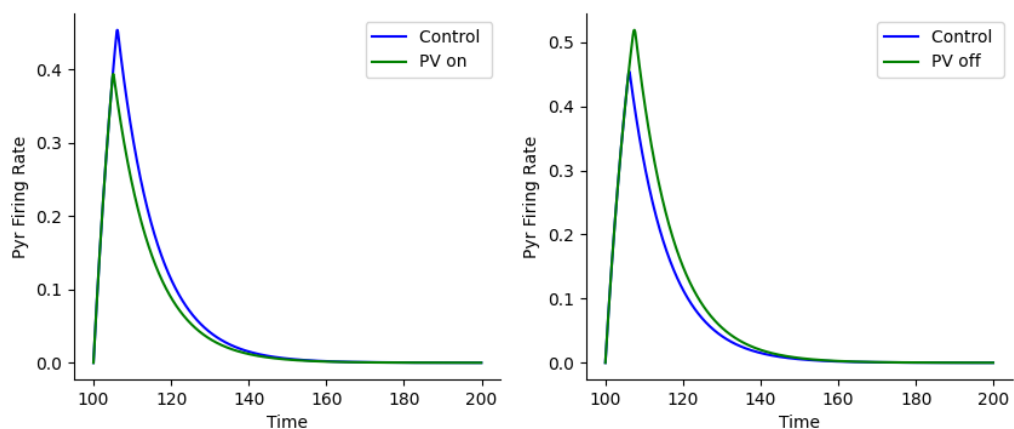


Figure 6. ReFig8: Activation of PVs enhanced feedforward connectivity in the model. Response of the cortical excitatory population to tones with (blue) and without (green) optogenetic manipulation. Left: optogenetic activation of the PV population. Right: optogenetic inactivation of the PV population.

Conclusion

In this work we provide a successful replication of the rate models from the article *A circuit model of auditory cortex* written by Youngmin Park and Maria N. Geffen [1]. We could qualitatively replicate all findings from the original article for the stimulus-specific adaptation, forward suppression and feedforward functional connectivity experiments with the exception of the predictions from optogenetic activation of the inhibitory cells in the forward suppression setting. Nevertheless, we consider this a successful replication. We would also like to highlight that Youngmin Park and Maria N. Geffen were very helpful in clarifying some issues with parameter discrepancies between text and tables in their article which led to initial failed replication attempts to be resolved quickly. We very much appreciated the quick responses and helpful conversations.

References

1. Y. Park and M. N. Geffen. "A circuit model of auditory cortex." In: **PLoS Computational Biology** 16.7 (2020), e1008016.
2. B. Ermentrout. "XPPAUT 5.0-the differential equations tool." In: **University of Pittsburgh, Pittsburgh** (2001).
3. C. Cakan, N. Jajcay, and K. Obermayer. "neurolib: a simulation framework for whole-brain neural mass modeling." In: **Cognitive Computation** (2021), pp. 1–21.
4. H. R. Wilson and J. D. Cowan. "Excitatory and inhibitory interactions in localized populations of model neurons." In: **Biophysical journal** 12.1 (1972), pp. 1–24.
5. M. Beierlein, J. R. Gibson, and B. W. Connors. "Two dynamically distinct inhibitory networks in layer 4 of the neocortex." In: **Journal of neurophysiology** 90.5 (2003), pp. 2987–3000.
6. M. V. Tsodyks, W. E. Skaggs, T. J. Sejnowski, and B. L. McNaughton. "Paradoxical effects of external modulation of inhibitory interneurons." In: **Journal of neuroscience** 17.11 (1997), pp. 4382–4388.
7. L. F. Abbott, J. Varela, K. Sen, and S. Nelson. "Synaptic depression and cortical gain control." In: **Science** 275.5297 (1997), pp. 221–224.
8. M. Wehr and A. M. Zador. "Synaptic mechanisms of forward suppression in rat auditory cortex." In: **Neuron** 47.3 (2005), pp. 437–445.
9. R. G. Natan, J. J. Briguglio, L. Mwilambwe-Tshilobo, S. I. Jones, M. Aizenberg, E. M. Goldberg, and M. N. Geffen. "Complementary control of sensory adaptation by two types of cortical interneurons." In: **Elife** 4 (2015), e09868.
10. T. S. Yarden and I. Nelken. "Stimulus-specific adaptation in a recurrent network model of primary auditory cortex." In: **PLoS computational biology** 13.3 (2017), e1005437.
11. A. Litwin-Kumar, R. Rosenbaum, and B. Doiron. "Inhibitory stabilization and visual coding in cortical circuits with multiple interneuron subtypes." In: **Journal of neurophysiology** 115.3 (2016), pp. 1399–1409.
12. E. A. Phillips, C. E. Schreiner, and A. R. Hasenstaub. "Cortical interneurons differentially regulate the effects of acoustic context." In: **Cell reports** 20.4 (2017), pp. 771–778.
13. L. S. Hamilton, J. Sohl-Dickstein, A. G. Huth, V. M. Carels, K. Deisseroth, and S. Bao. "Optogenetic activation of an inhibitory network enhances feedforward functional connectivity in auditory cortex." In: **Neuron** 80.4 (2013), pp. 1066–1076.